Received: 13 January 2022 | Revised: 02 May 2022 | Accepted: 02 May 2022

DOI: 10.1002/hep.32573

ORIGINAL ARTICLE

Multiomics identifies the link between intratumor steatosis and the exhausted tumor immune microenvironment in hepatocellular carcinoma

Hiroki Murai[1] | Takahiro Kodama[1] | Kazuki Maesaka[1] | Shoichiro Tange[2] | Daisuke Motooka[3] | Yutaka Suzuki[4] | Yasuyuki Shigematsu[5] | Kentaro Inamura[5] | Yoshihiro Mise[6] | Akio Saiura[6] | Yoshihiro Ono[7] | Yu Takahashi[7] | Yota Kawasaki[8] | Satoshi Iino[9] | Shogo Kobayashi[10] | Masashi Idogawa[2] | Takashi Tokino[2] | Tomomi Hashidate-Yoshida[11] | Hideo Shindou[11,12] | Masanori Miyazaki[13] | Yasuharu Imai[14] | Satoshi Tanaka[15] | Eiji Mita[15] | Kazuyoshi Ohkawa[16] | Hayato Hikita[1] | Ryotaro Sakamori[1] | Tomohide Tatsumi[1] | Hidetoshi Eguchi[10] | Eiichi Morii[17] | Tetsuo Takehara[1]

[1]Department of Gastroenterology and Hepatology, Osaka University Graduate School of Medicine, Suita, Japan

[2]Department of Medical Genome Sciences, Research Institute for Frontier Medicine, Sapporo Medical University School of Medicine, Sapporo, Japan

[3]Genome Information Research Center, Research Institute for Microbial Diseases, Osaka University, Suita, Japan

[4]Department of Computational Biology and Medical Sciences, Graduate School of Frontier Sciences, The University of Tokyo, Chiba, Japan

[5]Division of Pathology, Cancer Institute, Department of Pathology, Cancer Institute Hospital, Japanese Foundation for Cancer Research, Tokyo, Japan

[6]Department of Hepatobiliary-Pancreatic Surgery, Juntendo University School of Medicine, Tokyo, Japan

[7]Division of Hepatobiliary and Pancreatic Surgery, Cancer Institute Hospital, Japanese Foundation for Cancer Research, Tokyo, Japan

[8]Department of Digestive Surgery, Breast, and Thyroid Surgery, Graduate School of Medical Sciences, Kagoshima University, Kagoshima, Japan

[9]Department of Digestive Surgery, Kagoshima Principal Hospital, Kagoshima, Japan

[10]Department of Gastroenterological Surgery, Osaka University Graduate School of Medicine, Suita, Japan

[11]Department of Lipid Signaling, National Center for Global Health and Medicine, Tokyo, Japan

[12]Department of Lipid Medical Science, Graduate School of Medicine, The University of Tokyo, Tokyo, Japan

[13]Department of Gastroenterology and Hepatology, Osaka Police Hospital, Osaka, Japan

[14]Department of Gastroenterology and Hepatology, Ikeda Municipal Hospital, Osaka, Japan

[15]Department of Gastroenterology and Hepatology, National Hospital Organization Osaka National Hospital, Osaka, Japan

[16]Department of Hepatobiliary and Pancreatic Oncology, Osaka International Cancer Institute, Osaka, Japan

[17]Department of Pathology, Osaka University Graduate School of Medicine, Osaka, Japan

Abbreviations: ACVR2A, Activin A Receptor Type 2A; CAF, cancer-associated fibroblast; CTL, cytotoxic T-lymphocyte; CTNNB1, cadherin-associated protein beta 1; FFPE, formalin-fixed paraffin-embedded; GAGE, Generally Applicable Gene-set Enrichment; HT, hypertension; ICI, immune checkpoint inhibitor; IFN, interferon; IRB, Institutional Review Board; mALBI, modified albumin-bilirubin; mRECIST, modified Response Evaluation Criteria in Solid Tumors; NTP, nearest template prediction; OS, overall survival; PA, palmitic acid; PCA, principal component analysis; PD-1, programmed cell death protein 1; PD-L1, programmed death-ligand 1; PFS, progression-free survival; PMA, phorbol 12-myristate 13-acetate; PV, portal vein; ssGSEA, single-sample gene set enrichment analysis; TERT, telomerase reverse transcriptase; TIL, tumor-infiltrating lymphocyte; TIME, tumor immune microenvironment; TP53, tumor protein p53; αSMA, α smooth muscle actin.

Supplemental Digital Content is available for this article. Direct URL citations appear in the printed text and are provided in the HTML and PDF versions of this article on the journal's website, www.hepjournal.com.

Hiroki Murai and Takahiro Kodama contributed equally to this manuscript and share first authorship.

Correspondence
Tetsuo Takehara, Department of Gastroenterology and Hepatology, Osaka University Graduate School of Medicine, 2-2 Yamadaoka Suita, Osaka 565-0871, Japan.
Email: takehara@gh.med.osaka-u.ac.jp

Funding information
Core Research for Evolutional Science and Technology, Grant/Award Number: 21gm0910011; Japan Agency for Medical Research and Development, Grant/Award Number: JP21fk0210074, JP21fk0210091 and JP22fk0310524; Japan Society for the Promotion of Science, Grant/ Award Number: 16H06279; Ministry of Education, Culture, Sports, Science and Technology, Grant/Award Number: 20H03661; JSPS

Abstract

Background and Aims: Immunotherapy has become the standard-of-care treatment for hepatocellular carcinoma (HCC), but its efficacy remains limited. To identify immunotherapy-susceptible HCC, we profiled the molecular abnormalities and tumor immune microenvironment (TIME) of rapidly increasing nonviral HCC.

Approaches and Results: We performed RNA-seq of tumor tissues in 113 patients with nonviral HCC and cancer genome sequencing of 69 genes with recurrent genetic alterations reported in HCC. Unsupervised hierarchical clustering classified nonviral HCCs into three molecular classes (Class I, II, III), which stratified patient prognosis. Class I, with the poorest prognosis, was associated with TP53 mutations, whereas class III, with the best prognosis, was associated with cadherin-associated protein beta 1 (CTNNB1) mutations. Thirty-eight percent of nonviral HCC was defined as an immune class characterized by a high frequency of intratumoral steatosis and a low frequency of CTNNB1 mutations. Steatotic HCC, which accounts for 23% of nonviral HCC cases, presented an immune-enriched but immune-exhausted TIME characterized by T cell exhaustion, M2 macrophage and cancer-associated fibroblast (CAF) infiltration, high PD-L1 expression, and TGF-β signaling activation. Spatial transcriptome analysis suggested that M2 macrophages and CAFs may be in close proximity to exhausted CD8+ T cells in steatotic HCC. An in vitro study showed that palmitic acid-induced lipid accumulation in HCC cells upregulated PD-L1 expression and promoted immunosuppressive phenotypes of cocultured macrophages and fibroblasts. Patients with steatotic HCC, confirmed by chemical-shift MR imaging, had significantly longer PFS with combined immunotherapy using anti–PD-L1 and anti-VEGF antibodies.

Conclusions: Multiomics stratified nonviral HCCs according to prognosis or TIME. We identified the link between intratumoral steatosis and immune-exhausted immunotherapy-susceptible TIME.

INTRODUCTION

Liver cancer is the fourth leading cause of cancer-related death worldwide.[1] Hepatocellular carcinoma (HCC) is the most common type of primary liver cancer and is a heterogeneous disease with a variety of etiological factors.[2,3] Hepatitis C virus (HCV) is one of the major causes of HCC, and the prevalence of HCV-related HCC (HCV-HCC) has been decreasing worldwide owing to recent advances in surveillance and treatment.[4] Meanwhile, the prevalence of nonviral HCC is increasing rapidly, and it can have various causes, such as heavy drinking, NAFLD, and diabetes mellitus.[5] Understanding HCC diversity to develop targeted therapies will require unravelling the molecular mechanism underlying the carcinogenesis process. To this end, profiling of HCC at the genetic and transcriptomic levels has been performed over the past two decades.[6–8] However, the relationships between the molecular and clinicopathological features, especially in patients with nonviral HCC, have not been fully characterized, except the one recent report of the mutational characteristics of NASH-HCC.[9]

In recent years, immune checkpoint inhibitors (ICIs) have shown remarkable efficacy in various kinds of solid cancers.[10] These agents include monoclonal antibodies directed against cytotoxic T-lymphocyte–associated protein 4 (CTLA-4), programmed cell death protein 1 (PD-1), and its ligand PD-L1. In 2020, the IMbrave150 trial showed that anti–PD-L1 plus anti-VEGF therapy using atezolizumab plus bevacizumab significantly prolonged progression-free survival (PFS)

and overall survival (OS) compared with sorafenib in patients with unresectable HCC,[11] and combined immunotherapy has currently been in the spotlight as a treatment for HCC. Although it has become a front-line therapy for patients with advanced HCC, the response rate is approximately 30%; thus, more than half of patients will not derive much of a benefit. This could be due to the high heterogeneity of molecular abnormalities and the tumor immune microenvironment (TIME) of patients with HCC. In general, the TIME is stratified into immune-excluded, immune-active, and immune-exhausted subtypes based on the levels of tumor-infiltrating lymphocytes (TILs) and immune checkpoint expression.[12,13] A meta-analysis showed that TIL levels and PD-1/PD-L1 expression are positively associated with the response to ICIs in a variety of cancer types.[14,15] However, Pfister et al. have recently reported that nonviral HCC, particularly NASH-HCC, might be less responsive to immunotherapy, despite the presence of high levels of $CD8^+PD1^+$T cells, due to impaired immune surveillance,[16] suggesting the existence of a unique TIME in NASH-HCC. However, the heterogeneity of tumor immunity in nonviral HCC and its effect on the response to combined immunotherapy has not been clarified.

In this study, we performed molecular and immunological profiling of 113 patients with nonviral HCC through genomic and transcriptomic analyses. This multiomics approach was capable of stratifying patients with nonviral HCC according to their prognosis or TIME. We further identified a link between steatotic HCCs and the immune-enriched but immune-exhausted TIME. Mechanistically, we showed that lipid accumulation in HCC cells induced PD-L1 upregulation and promoted immunosuppressive changes in cocultured macrophages and fibroblasts. Last, we found that patients with steatotic HCC, identified by chemical-shift MR imaging, were susceptible to combined immunotherapy using anti–PD-L1 and anti-VEGF antibodies, suggesting that intratumor steatosis may be an imaging biomarker for predicting the efficacy of immunotherapy in HCC.

MATERIALS AND METHODS

Patient cohort for multiomics profiling

A total of 113 patients who underwent curative hepatic resection for nonviral HCC between 2005 and 2018 at The Cancer Institute Hospital of Japanese Foundation for Cancer Research and Kagoshima University Hospital were enrolled for the multiomics profiling study. These patients confirmed the absence of chronic liver disease, including viral hepatitis and autoimmune hepatitis. Snap-frozen HCC tissues were obtained for RNA and DNA sequencing, and formalin-fixed paraffin-embedded (FFPE) HCC and surrounding liver tissues were used for histological analysis. Among 113 patients with nonviral HCC, 54 patients who drink 30 g of alcohol or less for male patients and 20 g or less for female patients with fatty liver were categorized as having NAFLD-HCC. Patients with NAFLD-HCC were further classified into NASH-HCC or non–NASH-HCC based on the histological presence of steatosis and hepatocyte ballooning in the liver, as previously described.[17] Another 59 patients were categorized into three groups according to alcohol consumption as follows: 15 patients with heavy drinker (HD)-HCC who drink 60 g or more for male patients and 40 g or more for female patients/day, 13 patients with moderate drinker (MD)-HCC who drink 30–60 g for male patients and 20–40 g for female patients/day, and 31 patients with nondrinker (ND)-HCC who drink 30 g or less for male patients and 20 g or less for female patients/day (Figure S1). The amount of alcohol is the ethanol equivalent. The median observation period was 35 months. All patients provided written informed consent, and the study design was consistent with the principles of the Declaration of Helsinki. The protocol of the study using patient tissues was approved by the Institutional Review Board (IRB) committee at Osaka University Hospital (IRB No. 17097).

Patient cohort for response assessment of combined immunotherapy

Thirty patients who underwent abdominal MR imaging (including chemical-shift imaging [CSI]) before starting anti–PD-L1 plus anti-VEGF therapy using atezolizumab plus bevacizumab for HCC between October 2020 and September 2021 at Osaka University Hospital and six related hospitals were retrospectively enrolled in the immunotherapy study. The inclusion criteria were as follows: patients had measurable lesions in the liver, patients did not have marked iron deposition in the liver, and patients had their initial therapeutic response evaluated. The signal intensity of the largest tumor for each patient was acquired by drawing regions of interest from both in-phase and out-phase images at the same level. The fat fraction measured by CSI (FFCSI) was calculated using the following equation: FFCSI (%) = (in-phase intensity - opposed-phase intensity)/(2× in-phase intensity) × 100.[18] A tumor with FFCSI $\geq$ 10% was defined as steatotic HCC. During atezolizumab plus bevacizumab therapy, patients underwent dynamic contrast-enhanced computed tomography (CT) scans every 6 weeks to evaluate the therapeutic response. The response was assessed using the modified Response Evaluation Criteria in Solid Tumors (mRECIST). The median observation period was 5.4 months. All patients provided informed consent, and the study design was consistent with the principles of the Declaration of Helsinki. The protocol of the study using patient tissues was approved by the IRB committee at Osaka University Hospital (IRB No. 18201).

DNA and RNA extraction

Genomic DNA and total RNA were extracted from tissue specimens by using the DNeasy Blood & Tissue Kit (QIAGEN, Venlo, Netherlands) and RNeasy Mini Kit (QIAGEN), respectively, according to a previously reported procedure.[19] The integrity of the obtained DNA and RNA was confirmed by using a 2100 Bioanalyzer (Agilent Technologies, Santa Clara, CA).

RNA sequencing analysis

Total RNA was isolated from liver tissues as previously described.[20] Library preparation was performed using the TruSeq Stranded mRNA Sample Prep Kit (Illumina, San Diego, CA) on an Apollo Library Prep System (TaKaRa). Sequencing was performed on an Illumina HiSeq 3000 platform in 75-base single-end mode. Sequenced reads were mapped to the human reference genome sequence (hg19) using TopHat v2.1.1. Inter-sample normalization was performed using the TMM method for clustering analysis and the RLE method for the differentially expressed gene analysis.

Genome sequencing analysis

On library preparation, custom PCR primer sets for amplicon sequencing targeting the coding regions of 69 genes and TERT promoter regions were designed by Ion AmpliSeq Designer (Table S1). The genomic DNA extracted from 55 pairs of tumor and normal tissues was used for library preparation. Methods for library preparation, sequencing, alignment to the human reference genome sequence, and single nucleotide variant and copy number variation analyses are described in detail in the Supporting Methods.

Spatial transcriptomics on the Visium platform

A single steatotic HCC sample was embedded in optimal cutting temperature compound (TissueTek Sakura) in a 10 mm × 10 mm cryomold at -80°C and sectioned at a thickness of 10 μm (Leica CM3050 S). Libraries for Visium were prepared according to the Visium Spatial Gene Expression User Guide. Tissue was permeabilized for 3 min, which was identified as the optimal time in tissue optimization time course experiments. Libraries were sequenced on a NovaSeq 6000 System (Illumina) using the NovaSeq S4 Reagent Kit (200 cycles, 20,027,466, Illumina) at a sufficient sequencing depth. Raw FASTQ files and histology images were processed using Space Ranger software v1.2.1 (https://support.10xgenomics.com/spatial-gene-expression/software/pipelines/latest/installation). To visualize spatial expression using histological images, the raw Visium files for each sample were read into Loupe Browser software v4.0.0 (https://support.10xgenomics.com/spatial-gene-expression/software/downloads/latest). We obtained mean sequence read counts of 288,702 and identified median genes of 3300 per spot. The median-normalized average of a gene in a cluster is calculated as the mean of observed UMI counts normalized by the size factor for each cell in the representative cluster.

Statistical analysis

The data are expressed as the means ± standard deviations. Statistical analysis was performed with Mann–Whitney *U* tests to assess differences between unpaired groups. One-way analysis of variance followed by the Kruskal–Wallis test was performed for multiple comparisons. Fisher's exact test was used to analyze categorical data. Correlations were assessed using the Pearson product–moment correlation coefficient. The Kaplan–Meier method and log-rank test were used to analyze differences in OS or PFS. Univariate and multivariate logistic regression analyses were used to analyze factors associated with immune class in nonviral HCCs. Odds ratios and 95% confidence intervals are shown. A p value <0.05 was considered to indicate statistical significance unless otherwise indicated. Prism version 8.4.2 for Mac (GraphPad Prism, RRID:SCR_002798, San Diego, CA) and SPSS software version 24 (IBM Corporation, Armonk, NY) were used for the analyses.

RESULTS

Multiomics classifies nonviral HCCs into three prognostically stratified subgroups

A total of 113 patients who underwent hepatic resection for nonviral HCC were enrolled in this study. Clinical background information is provided in Table S2. The 3-year and 5-year survival rates after hepatic resection were 80% and 67%, respectively (Figure S2). Tumor RNA sequencing was performed to understand the molecular abnormalities of nonviral HCCs. Unsupervised hierarchical clustering analysis of transcriptomics classified 113 patients with nonviral HCC into three molecular classes (class I, II, and III) (Figure 1A). Patients with Class I had the poorest prognosis, whereas patients with Class III had the best prognosis (Figure 1B). Regarding the clinical characteristics, background liver disease was not associated with any classes (Figure S3), but Class I was characterized by high serum levels of alpha-fetoprotein and des-γ-carboxy prothrombin, a larger tumor size, and the

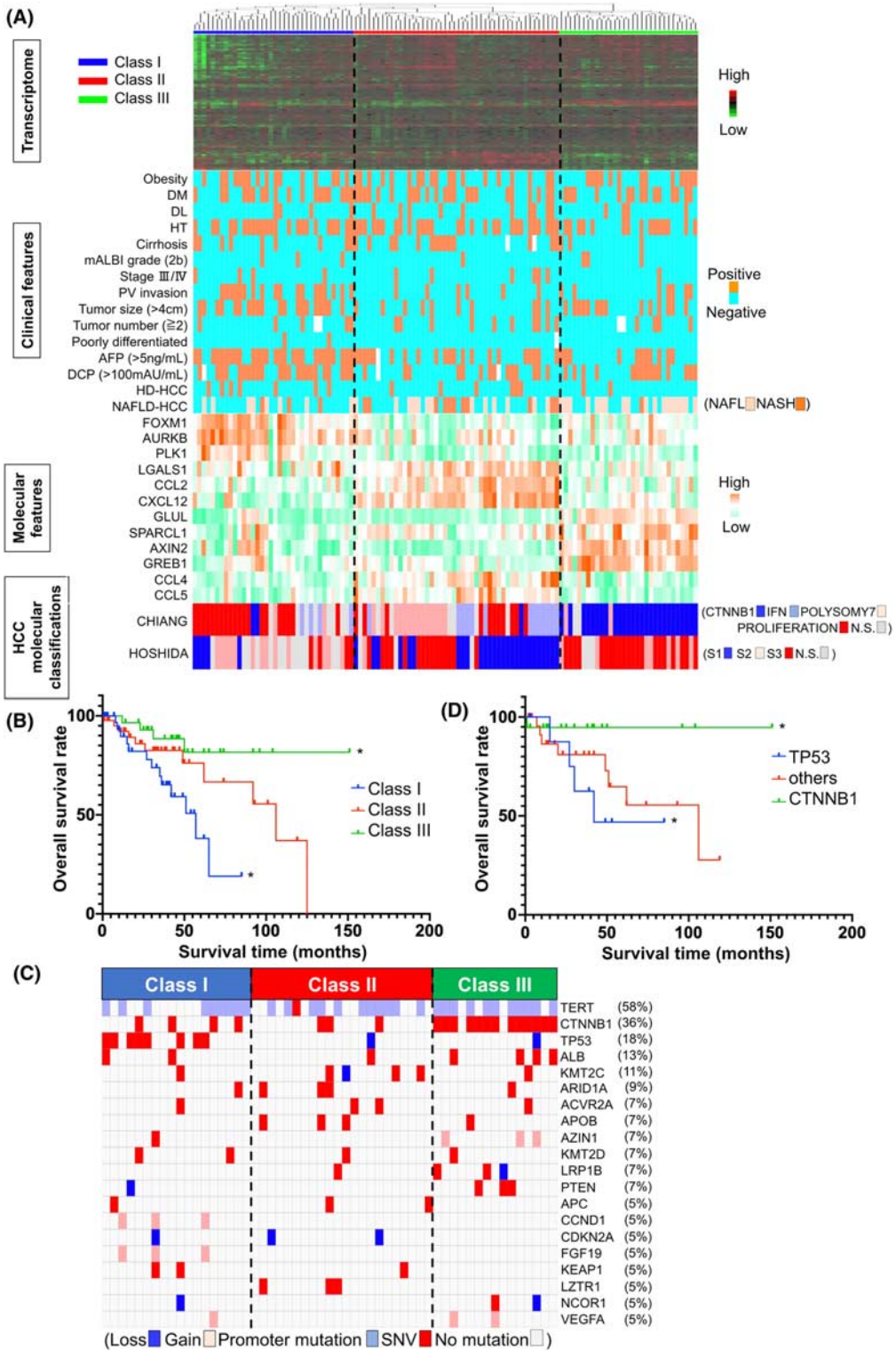

FIGURE 1 Multiomics classifies nonviral HCCs into three prognostically stratified subgroups. (A) Transcriptomic classification of nonviral HCCs. Unsupervised hierarchical clustering analysis of gene expression identified three classes: Class I (blue, $n = 36$), Class II (red, $n = 46$), and Class III (green, $n = 31$). Clinicopathological features are shown with missing values in white. The panel of molecular features is a heatmap displaying the relative expression levels of representative genes for each cluster. The panel of molecular classifications is a heatmap displaying the comparison of aggregate scores with gene sets associated with the previously defined molecular classifications. DM, DL, HT, and PV represent diabetes mellitus, dyslipidemia, hypertension, and portal vein, respectively. (B) Kaplan–Meier analysis of patients stratified by molecular class (* $p < 0.05$, Class I vs. Class II and Class III vs. others). (C) Cancer genome sequence analysis of 55 nonviral HCC patients. Only genes with a mutation frequency of 5% or more are presented in the order of molecular subtype. The results of all the genes are presented in Figure S5. (D) Kaplan–Meier analysis of patients with nonviral HCC stratified by genomic abnormality (*$p < 0.05$, TP53 vs. cadherin-associated protein beta 1 [CTNNB1]).

presence of portal vein (PV) invasion (Table S3). The multivariate Cox proportional hazard analysis showed that Class I and heavy drinking were independent poor prognostic factors (Table S4). Class I showed the enrichment of cell cycle- and mitosis-related gene sets in the GAGE analysis with the upregulation of FOXM1 and Aurora Kinase B (AURKB) (Figures 1A, S4A, and S5). Class III showed the depletion of immune cell activation-related gene sets in GAGE analysis and upregulation of genes in the WNT-β–catenin signaling pathway, including GLUL, SPARCL1, axis inhibition protein 2 (AXIN2) and GREB1, and downregulation of genes involved in dendritic cell migration to tumor cells, including CCL4 and CCL5 (Figures 1A, S4B, and S5). Regarding previously reported molecular classifications,[7,8] Class I was linked to the subclasses of PROLIFERATION in Chiang's molecular classification (Figure 1A, Table S5). Class II was linked to the subclasses of IFN in Chiang's classification and S1 in Hoshida's classification (Figure 1A, Table S5). Class III was linked to the subclasses of CTNNB1 in Chiang's classification and S3 in Hoshida's classification (Figure 1A, Table S5).

We next conducted cancer genome sequencing of 55 patients with nonviral HCC using gene panels detecting abnormalities in 69 genes in which recurrent genetic alterations were previously reported in HCC.[21] Somatic mutations were detected in 50 of the 55 samples and frequently observed in the TERT promoter region (58%), CTNNB1 (36%), and TP53 (18%) (Figures 1C, S6). Integrative analysis revealed close associations of Class I with the TP53 mutation ($p < 0.05$) and Class III with the CTNNB1 mutation ($p < 0.05$) (Figure 1C, Table S6). Patients with nonviral HCC with TP53 mutations had the poorest prognosis, whereas patients with nonviral HCC with CTNNB1 mutations had the best prognosis (Figure 1D). Regarding the background liver disease, patients with NASH-HCC exhibited significantly higher mutation rates of KMT2C (42.8% vs. 6.3% of patients with HCC of other etiologies) and Activin A Receptor Type 2A (ACVR2A) (29.5% vs. 4.2% of patients with HCC of other etiologies) (Figure S7A).

We then performed an external validation of our molecular classification in 180 patients with nonviral HCC in the TCGA database and confirmed that Class I had a high TP53 mutation rate with poorest prognosis and Class III had a high CTNNB1 mutation rate in TCGA cohort (Figure S7B,C).

Classification of nonviral HCCs based on the TIME

Next, to classify nonviral HCCs based on the TIME, we performed NTP analysis of tumor transcriptomes and identified the immune class that was reported to be a subtype characterized by strong intratumoral immune cell infiltration in HCC.[13] Forty-three out of 113 tumors were categorized into the immune class and showed significantly higher levels of estimated total intratumor immune cells and cytotoxic T-lymphocytes (CTLs) by CIBERSORT analysis (Figure 2A,B). The immune class showed the enrichment of tumors in Class II and significantly less frequent mutations of CTNNB1 (Figure 2C,D, Tables S7 and S8). Consistently, nonviral HCCs with CTNNB1 mutation showed significantly lower levels of intratumoral immune cell infiltration (Figure 2E), which is in agreement with previous reports.[22]

Steatotic HCC presents an immune-enriched but immune-exhausted TIME

We then searched for the clinicopathological factors that characterize the immune class and found that steatosis in HCC was strongly associated with the immune class (Table S9). Indeed, steatotic HCC, which accounts for 23% of nonviral HCC cases (Figure 3A), contained significantly higher levels of total intratumor immune cells than nonsteatotic HCC (Figures 3B,C, S8). Interestingly, ssGSEA and pathway analysis showed significantly higher levels of the T cell exhaustion signature and stromal signature together with activation of TGF-β signaling in steatotic HCC (Figure 3C,D), all of which were characteristics of exhaustion of tumor immunity.[23–26] Consistently, steatotic HCC also showed the upregulation of a variety of immune checkpoints and transcription factors involved in T cell exhaustion and markers of cancer-associated fibroblasts (CAFs) (Figures 3E and S9). In addition, the CIBERSORT analysis showed the substantial infiltration of M2 macrophages in steatotic HCC, together with the upregulation of cytokines and chemokines involved in M2 polarization of macrophages and immunosuppression (Figures 3C,E,F and S9). The immunohistochemical analysis confirmed the upregulation of PD-L1 in GPC3-positive HCC cells and substantial infiltration of CAFs and M2 macrophages in nonviral HCC samples (Figures 3G–J and S10). Overall, steatotic HCC presented an immune-enriched but immune-exhausted TIME characterized by T cell exhaustion, infiltration of M2 macrophages and CAFs, high PD-L1 expression, and TGF-β signaling activation.

Exhausted T cells, M2 macrophages, and CAFs interact in close proximity and constitute the immune-exhausted TIME in steatotic HCC

To further characterize the immune-exhausted TIME in steatotic HCC, we examined the topography of M2 macrophages, CAFs and CTLs in steatotic HCC by

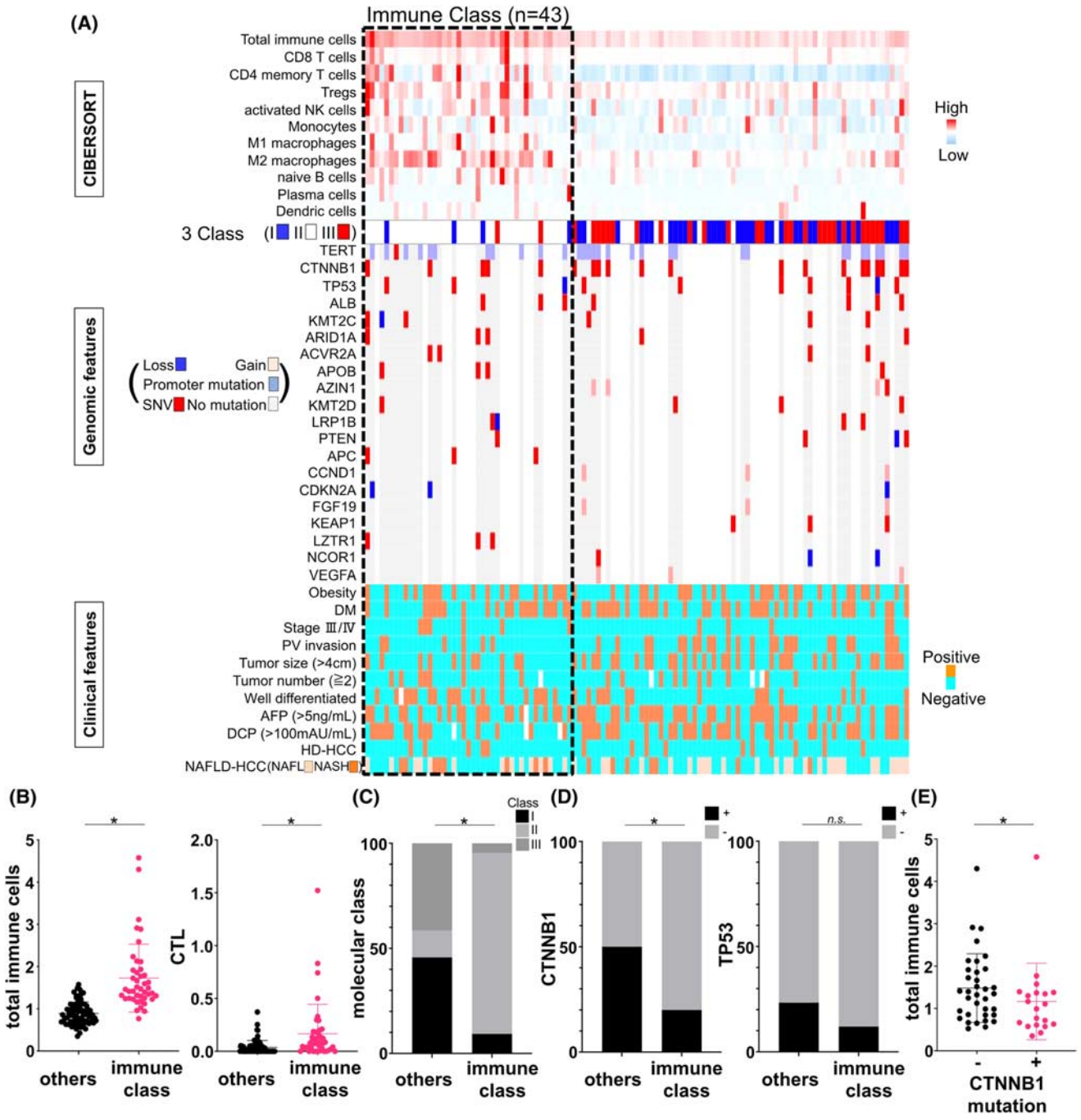

FIGURE 2 Classification of nonviral HCCs based on the TIME. (A) NTP analysis of tumor transcriptomes identified 43 out of 113 tumors as immune class in nonviral HCCs. The panel of CIBERSORT is a heatmap displaying the estimated infiltrating scores of each immune cell. The panel of three classes is a heatmap displaying the comparison with the unsupervised hierarchical clustering shown in Figure 1A. Genomic features and clinicopathological features are shown with missing values in white. (B) Comparison of the CIBERSORT score for total immune cells and cytotoxic T cells between the immune class and the other. (*$p < 0.05$). (C) Comparison of the percentage of each molecular class between the immune class and the other. The immune class had a significantly higher percentage of Class II (*$p < 0.05$). (D) Comparison of the percentage of cadherin-associated protein beta 1 (CTNNB1) or TP53 mutations between the immune class and the other (*$p < 0.05$). (E) Comparison of the CIBERSORT score for total immune cells between HCCs with and without CTNNB1 mutation (*$p < 0.05$).

spatial transcriptomics on the Visium platform. The tumor section was divided into 1768 spots, and transcriptomic data were obtained from each spot. First, graph-based clustering divided all the spots into six clusters, with high expression of immune cell populations in cluster 2 (Figure 4A–C). ssGSEA showed that the stromal signature and T cell exhaustion signature were enhanced in cluster 2 (Figure 4C). We extracted CD8A and NR4A1 double-positive spots as spots containing exhausted CTLs and

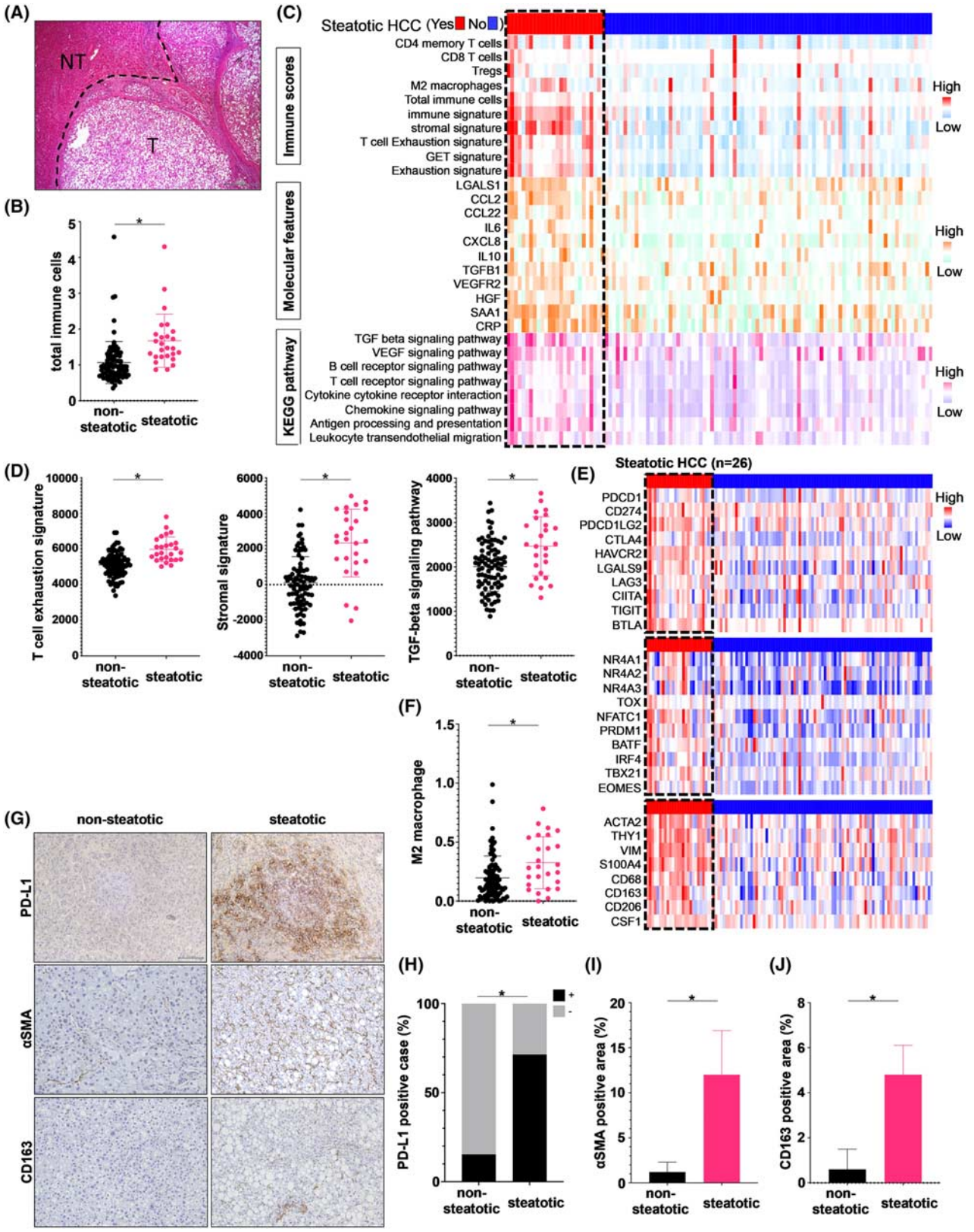

found that almost half of these spots were included in cluster 2 (Figure 4D). Then, we compared transcriptomic profiles between spots with or without exhausted CTLs (Figure 4E). We found increased expression of the M2 macrophage marker CD163 and the CAF marker VIM in addition to elevated TGFB1

FIGURE 3 Steatotic HCC presents an immune-enriched but immune-exhausted TIME. (A) A representative image of steatotic HCC. T and NT stand for tumor and nontumor, respectively. (B) Comparison of the CIBERSORT score for total immune cells between steatotic and nonsteatotic HCC samples (*$p < 0.05$). (C) Twenty-six out of 113 cases were identified as steatotic HCC. The panel of immune scores is a heatmap displaying the enrichment scores of immune-related gene signatures and the CIBERSORT scores. The panel of molecular features is a heatmap displaying the relative expression levels of representative genes enhanced in steatotic HCC. The panel of KEGG pathways is a heatmap displaying the enrichment scores of representative signaling pathways enhanced in steatotic HCC. (D) Comparison of the enrichment scores for the T cell exhaustion signature, stromal signature, and TGF-beta signaling pathway between steatotic and nonsteatotic HCC samples (*$p < 0.05$). (E) Heatmap displaying the relative expression levels of representative genes for inhibitory immune checkpoint molecules (top), transcription factors involved in T cell exhaustion (middle) and markers of cancer-associated fibroblasts (CAFs) and M2 macrophages (bottom). (F) Comparison of the CIBERSORT score for M2 macrophages between steatotic and nonsteatotic HCC samples (*$p < 0.05$). (G) Representative images of immunohistochemistry staining for PD-L1, αSMA and CD163. (H-J) Comparison of the percentage of PD-L1-positive HCC samples (H) and positive areas of αSMA (I) and CD163 (J) staining between steatotic HCC and nonsteatotic HCC ($n = 5$–13 samples per group, *$p < 0.05$).

levels in the spots with exhausted CTLs (Figure 4F). These results suggested that M2 macrophages and CAFs might produce TGF-β and promote exhaustion of surrounding CTLs in close proximity, forming an immune-exhausted TIME in steatotic HCC. The close proximity of CTLs to M2 macrophages and CAFs was also confirmed by the immunohistochemical staining of the steatotic HCC tissues (Figure S11).

PA-induced lipid accumulation in tumor cells may promote immunosuppression in steatotic HCC

We then investigated the mechanistic link between intratumor steatosis and the immune-exhausted TIME in HCC. Therefore, we first performed lipidomics-based total fatty acid profiling and found that PA levels were significantly higher in steatotic HCC samples than in nonsteatotic HCC tissues (Figure S12). We thus examined the effect of PA accumulation on HCC cells in vitro. PA supplementation in Hep3B cells induced lipid accumulation (Figure 5A) and upregulated PD-L1 expression at both the mRNA and surface protein levels (Figure 5B,C), together with the upregulation of Colony Stimulating Factor 1 (CSF1), C-X-C Motif Chemokine Ligand 8 (CXCL8), and TGF-β1 at both the mRNA and secreted protein levels (Figure 5D,E), all of which are known to promote the M2 polarization of macrophages and/or activate CAFs.[27–29] The upregulation of these genes on PA supplementation was also verified in two other HCC cell lines, Huh7 and SNU387 cells (Figure S13A,B). Mechanistic analyses suggested that JNK and Stat3 signaling pathways were at least partially involved in PA-induced upregulation of PD-L1 and CXCL8, but not of CSF1 and TGFB1 (Figure S14A–D). We further investigated the effect of PA accumulation in tumor cells on surrounding macrophages and fibroblasts in vitro. PA-treated Hep3B cells upregulated the expression levels of *CD206* and *IL10* in a cocultured human macrophage cell line (Figure 5F) and *TGFB1* in a cocultured human hepatic stellate cell line (Figure 5G). Upregulation of these immunosuppressive cytokines and chemokines was also observed in steatotic HCC in vivo (Figure 5H). These data suggested that PA accumulation in tumor cells promotes immunosuppression, which may contribute to the development of an immune-exhausted TIME in steatotic HCC.

Patients with steatotic HCC are susceptible to combined immunotherapy using atezolizumab plus bevacizumab

Because of the immune-enriched but immune-exhausted TIME with high PD-L1 expression in steatotic HCC, we hypothesized that steatotic HCC may be susceptible to ICI treatment. To investigate this hypothesis, we first aimed to identify steatotic HCC by MRI because most patients with advanced HCC who undergo systemic pharmacotherapy do not undergo tumor biopsy in general practice. A strong positive correlation was observed between the levels of histological lipid deposition and FFCSI measured by chemical-shift MRI in 20 surgically resected HCCs (Figure S15), confirming that MRI is a reliable tool to identify steatotic HCC.[18] We then retrospectively analyzed 30 patients with advanced HCC treated with atezolizumab plus bevacizumab. Seven out of 30 patients were classified as steatotic HCC based on chemical-shift MRI (Figure 6A,B). No significant difference in clinical backgrounds was observed between patients with steatotic and nonsteatotic HCC (Table S10). None of the patients with steatotic HCC showed disease progression during the 5.4-month observation period. Consequently, patients with steatotic HCC experienced a significantly longer PFS than patients with nonsteatotic HCC (Figure 6C). These findings suggested that patients with steatotic HCC may be susceptible to ICI therapy and that intratumor steatosis may be an imaging biomarker predicting the efficacy of ICI therapy in HCC.

DISCUSSION

In this study, to clarify the molecular and immunological features of nonviral HCCs, we performed multiomics profiling. Molecular classification stratified nonviral

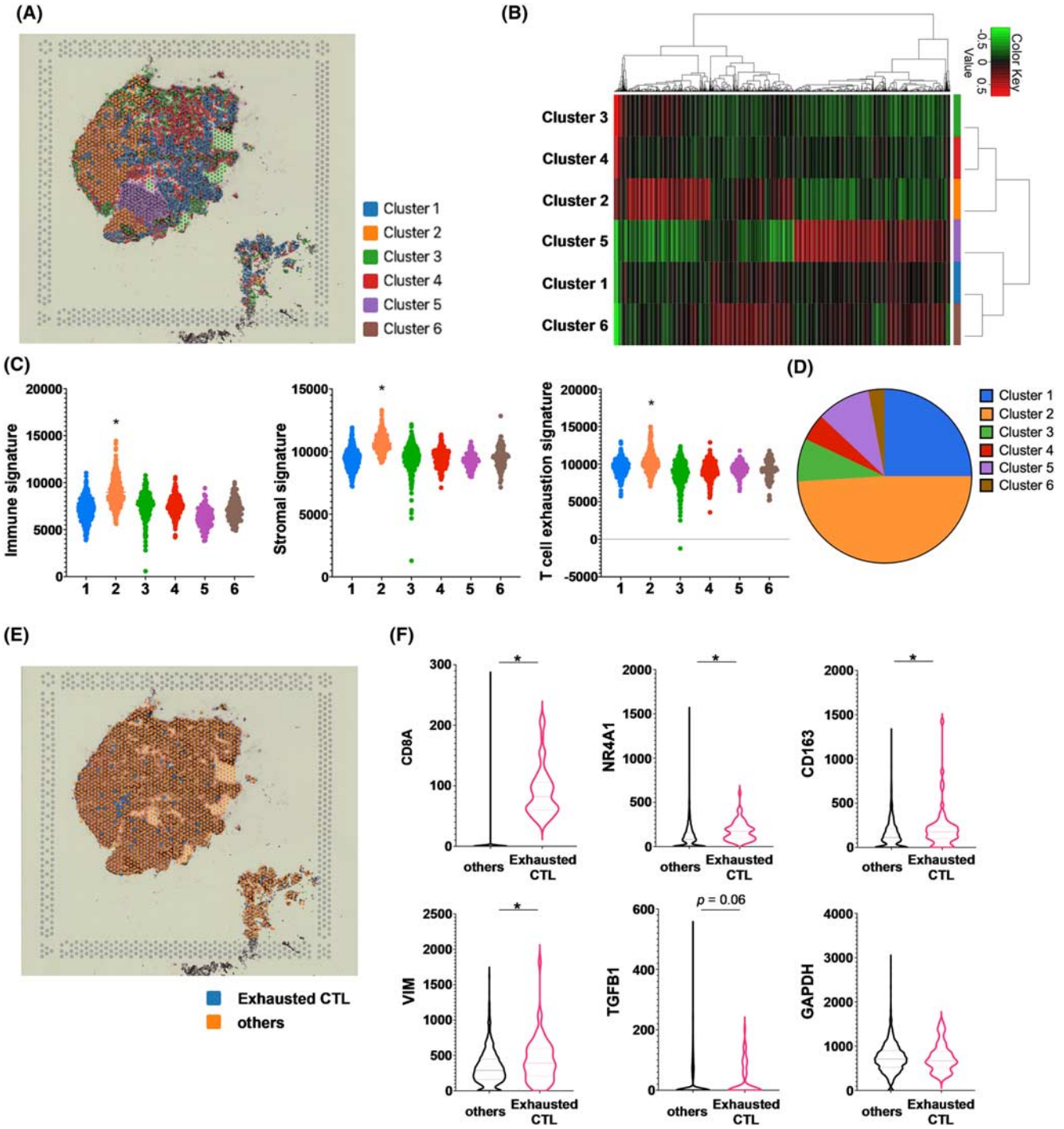

FIGURE 4 Exhausted T cells, M2 macrophages, and cancer-associated fibroblasts (CAFs) interact in close proximity and constitute the immune-exhausted TIME in steatotic HCC. (A) Graph-based clustering of spatial transcriptomic data of steatotic HCC tissue in the Visium platform. (B) Heatmap of transcriptomic data by cluster. The graph-based hierarchical clustering analysis divided all the spots into six clusters. (C) Enrichment scores for the immune signature, stromal signature and T cell exhaustion signature in each cluster (*$p < 0.05$, cluster 2 vs. others). (D) A pie chart showing the percentage of exhausted cytotoxic T-lymphocyte (CTL) spots defined as CD8A-positive and NR4A1-positive in each cluster. (E) Location of the spots containing exhausted CTLs on the section. (F) Violin plots displaying the expression levels of M2 macrophage markers, CAF markers and TGFB1 in the exhausted CTL spots and the rest (*$p < 0.05$).

HCCs into three classes that were strongly associated with patient prognosis and corresponding driver gene abnormalities. They include two major HCC molecular classes previously defined based on viral HCCs, including the "proliferative" class with TP53 mutation and poor prognosis[30–32] and the "CTNNB1" class with the immune-"cold" phenotype and good prognosis.[8,22] We also found that genomic abnormalities in major driver genes in patients with nonviral HCC were similar to those reported in patients with viral HCC.[21] On the

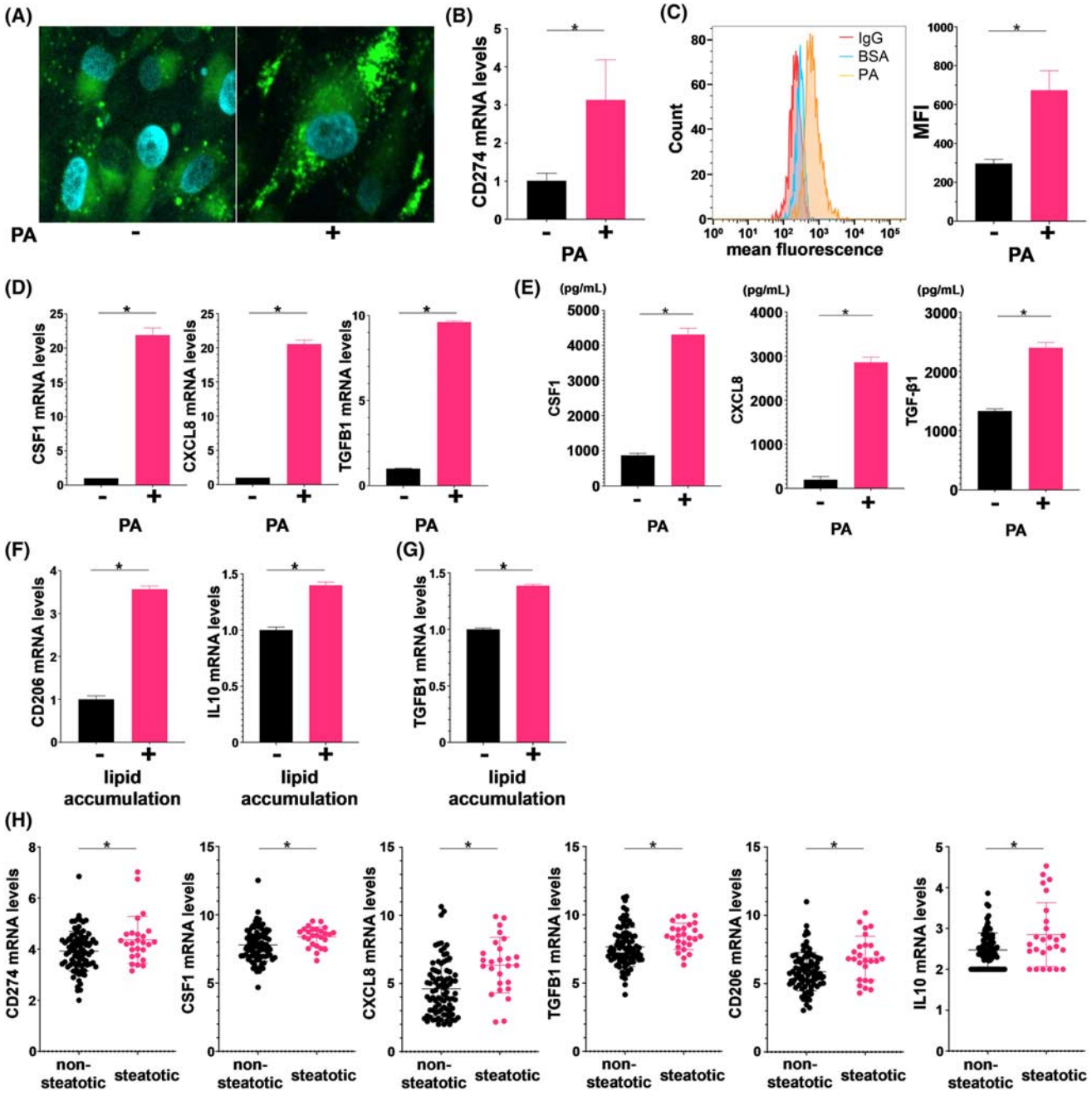

FIGURE 5 PA-induced lipid accumulation in tumor cells may promote immunosuppression in steatotic HCC. (A) BODIPY-stained images in Hep3B cells 24 h after bovine serum albumin (BSA) or palmitic acid (PA) supplementation. (B) Relative mRNA levels of *CD274* in Hep3B cells 24 h after BSA or PA supplementation ($n = 3$ each and $^*p < 0.05$). (C) Flow cytometry analysis of CD274 protein levels in Hep3B cells 24 h after BSA or PA supplementation shown as a histogram (left) and mean fluorescence intensity (MFI) (right) ($n = 3$ each and $^*p < 0.05$). (D) Relative mRNA levels of *Colony Stimulating Factor 1* (*CSF1*), *C-X-C Motif Chemokine Ligand 8* (*CXCL8*) and *TGFB1* in Hep3B cells 24 h after BSA or PA supplementation ($n = 3$ samples each and $^*p < 0.05$). (E) Secreted levels of the CSF1, CXCL8 and TGF-β1 proteins in the supernatant of Hep3B cells 24 h after BSA or PA supplementation ($n = 3$ samples each and $^*p < 0.05$). (F) Relative *CD206 and IL10* mRNA levels in macrophages after 3 days of coculture with BSA- or PA-supplemented Hep3B cells ($n = 3$ samples each and $^*p < 0.05$). (G) Relative *TGFB1* mRNA levels in LX-2 cells after 3 days of coculture with BSA- or PA-supplemented Hep3B cells ($n = 3$ samples each and $^*p < 0.05$). (H) Relative *CD274, CSF1*, *CXCL8*, *TGFB1, CD206*, and *IL10* mRNA levels in steatotic and nonsteatotic HCC samples ($^*p < 0.05$).

other hand, our nonviral HCC cohort contains 38% of patients classified into the immune class, which was higher than the 25% of patients classified into the immune class in the previously reported original cohort, where 2/3 of patients had viral HCC,[13] suggesting an unprecedented link between etiological differences and immunokinetics in HCC.

Pinyol et al. have recently reported the molecular features of 53 NASH-HCC samples.[9] Their genomic analysis showed that NASH-HCC samples had

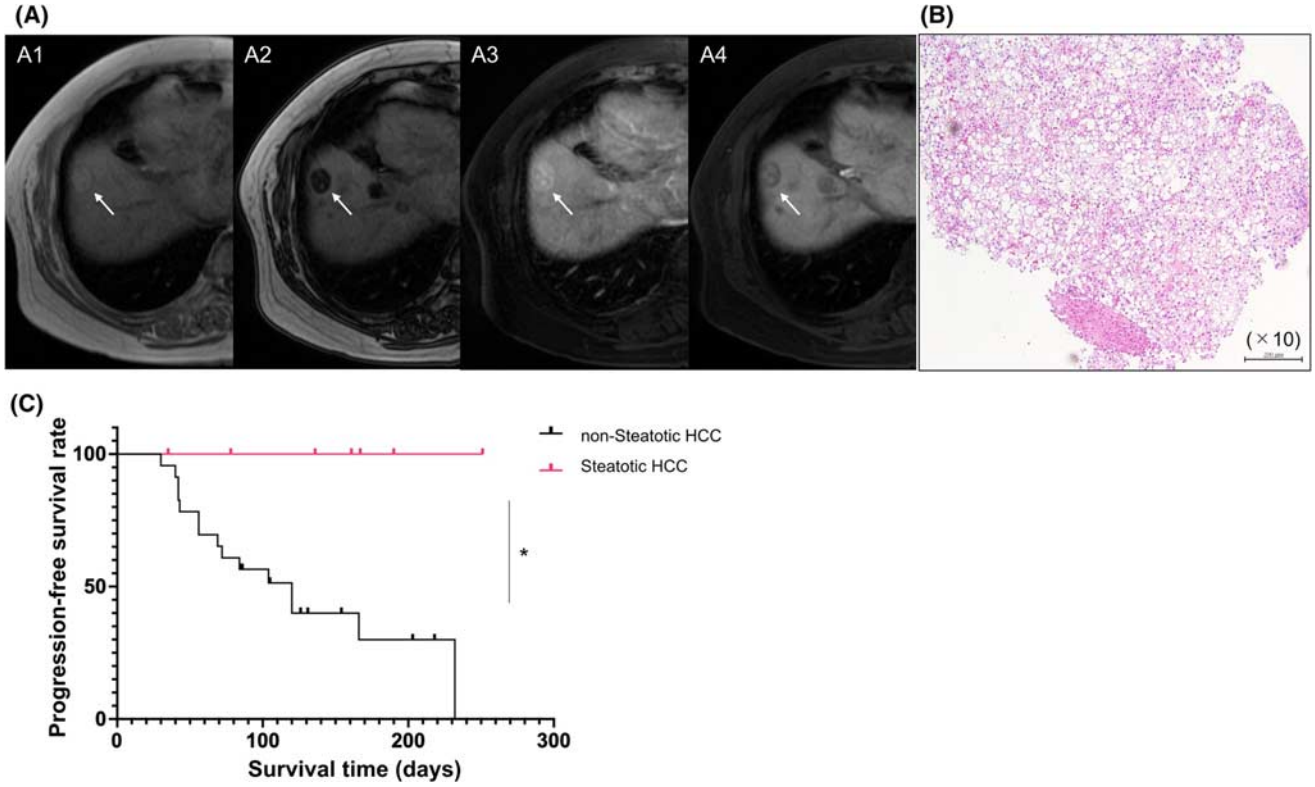

FIGURE 6 Patients with steatotic HCC are susceptible to combined immunotherapy using atezolizumab plus bevacizumab. (A,B) Representative MR and HE images of steatotic HCC. (A) A1; In-phase T1-weighted gradient-echo MR image shows a well-defined hyperintense mass just below the diaphragm aspect of hepatic segment VIII (arrow). A2; Opposed-phase T1-weighted gradient-echo MR image corresponding to A1 reveals a drop in the signal intensity of the tumor (arrow). A3; Hepatic arterial phase of gadolinium ethoxybenzyl diethylenetriamine pentaacetic acid (Gd-EOB-DTPA)-enhanced MR image shows arterial enhancement of the tumor (arrow). A4; 20-min hepatobiliary phase of Gd-EOB-DTPA–enhanced MR image reveals a drop in the signal intensity of the tumor (arrow). (B) HE images of the tumor biopsy specimen. (C) Kaplan–Meier analysis of the PFS of patients stratified by the presence or absence of steatosis in HCC (*$p < 0.05$).

significantly higher rates of ACVR2A mutations (10%) and lower rates of TP53 mutations (18%) than HCCs of other etiologies, consistent with the results from our small NASH-HCC cohort showing high ACVR2A mutation rates (29%) and low TP53 mutation rates (14%) (Figure S7A). Their transcriptomic analysis revealed a lower prevalence of the CTNNB1 molecular subclass in NASH-HCCs, which was also observed in our cohort (6.7% in NASH-HCC vs. 30% in HCC of other etiologies) (Figure 1A). Their immunological analysis showed that 30% of NASH-HCCs belonged to the immune class, the frequency of which was lower than that in our cohort (53%) (Figure 2A), but NASH-HCCs were characterized by an immunosuppressive cancer field in the surrounding liver. Collectively, these two reports revealed the unique molecular features of NASH-HCC.

Through the investigation of the TIME in nonviral HCCs, we identified a link between intratumoral steatosis and the immune-exhausted TIME. In recent years, several studies have reported that lipid droplets accumulated in cancer cells are involved in cell–cell cross-talk in the TIME.[33–37] However, the literature includes both protumorigenic and antitumorigenic functions, and thus, their roles are complex and appear to be context-dependent.[33,36,38] Furthermore, there are no reports of a causal relationship between lipid accumulation and immune checkpoints. In the present in vitro study, we demonstrated that lipid accumulation in HCC cells upregulated membranous PD-L1 expression and promoted immunosuppressive changes in cocultured macrophages and fibroblasts. Moreover, spatial transcriptome analysis suggested the close association of M2 macrophages and CAFs with exhausted CTLs in steatotic HCCs in vivo. These findings suggested that intratumoral steatosis may furnish immune-exhausted TIMEs in HCC. Calderaro et al. have previously classified HCC into six subgroups based on the pathological and molecular features.[39] Among them, the G4 subgroup is characterized by steatohepatic HCC, immunohistochemical C-Reactive Protein (CRP) expression and high levels of inflammatory cell infiltration with less frequent CTNNB1 and TP53 mutations. Similarly, our steatotic HCC samples showed a high degree of inflammatory cell infiltration (Figure 3B), high *CRP* mRNA levels (Figure 3C), and lower mutation rates of CTNNB1 (16.7% in steatotic HCCs vs. 41.9% in nonsteatotic HCCs) and TP53 (0%

in steatotic HCCs vs. 23.3% in nonsteatotic HCCs). Therefore, although the authors did not evaluate the immune exhaustion status of the G4 subgroup in their study, our steatotic HCC samples may be closely related to the G4 subgroup.

We evaluated the clinical significance of steatotic HCC. ICIs conceptually reinvigorate exhausted effector T cells and are known to be more effective in cancers with high tumor–infiltrated CTL and PD-L1 expression.[15] Because steatotic HCC is characterized by an immune-exhausted TIME with high PD-L1 expression, we hypothesized the high susceptibility of steatotic HCCs to ICI treatment. To study this hypothesis, it was necessary to seek a noninvasive method to detect steatotic HCC because patients with unresectable advanced HCC who are eligible for immunotherapy are often diagnosed through dynamic CT or MRI and treated without tumor biopsy. We found that chemical-shift MRI successfully identified steatotic HCC. Therefore, our study sheds light on the potential utility of MRI as a noninvasive imaging biomarker reflecting the TIME of HCC. It is also clinically applicable because gadolinium ethoxybenzyl diethylenetriamine pentaacetic acid (Gd-EOB-DTPA)–enhanced MRI is often used to diagnose HCC even in the advanced setting. Importantly, despite the small cohort, patients with steatotic HCC, who were identified by chemical-shift MRI, experienced significantly longer PFS than patients with nonsteatotic HCC after treatment with anti–PD-L1 plus anti-VEGF therapy. These results also suggested that intratumor steatosis may be an imaging biomarker predicting the efficacy of ICI therapy for advanced HCC.

Pfister et al. have recently reported that ICI therapy might be less effective against nonviral HCCs compared to viral HCCs.[16] They proposed a potential mechanism by which $PD1^{+}CD8^{+}$ T cells, which are present at higher levels in the liver of patients with NASH, induced liver injury on PD-1 blockade and instead promoted hepatocarcinogenesis. Because we did not analyze the immune microenvironment of adjacent tumor tissue in our present study, we did not clearly determine whether this immunological feature was present in our cohort. However, a larger percentage of patients with HCC presenting with NASH in our cohort had steatotic HCC, and thus they are predicted to respond to immunotherapy compared to patients with other etiologies (53% of patients with NASH-HCC vs. 18% of patients with HCC of other etiologies). This result is consistent with a previous report showing that tumor steatosis preferentially occurs in patients with metabolic syndrome.[40] We also did not observe significant differences in response rates (33% of patients with nonviral HCC vs. 20% of patients with viral HCC) and PFS (3.5 months for patients with nonviral HCC vs. 3.5 months for patients with viral HCC) between patients in our cohort with nonviral and viral HCC who were treated with Atezo/Bev therapy, although the sample size is very small. Additionally, a favorable therapeutic effect of anti–PD-L1/VEGF therapy on nonviral HCC was reported in the ORR subgroup analysis of the IMbrave150 study[11] and anti–PD-L1/anti–CTLA-4 therapy was effective regardless of etiology in the CheckMate-040 study.[41] Collectively, the effect of NASH etiology on the efficacy of immunotherapy in patients with HCC remains unclear and may be clarified as larger sets of real-world evidence become available.

Our study has several limitations. First, our cohort for the multiomics analysis only includes patients who underwent surgical resection of HCC. Therefore, we did not clearly determine whether our molecular classification is also applicable to patients with unresectable advanced HCC. Second, the size of our cohort of patients with advanced HCC who were treated with combination immunotherapy is small, and a future validation study is needed. Third, we did not perform in vivo validation of the relationship between lipid accumulation and immune exhaustion using animal models.

In conclusion, multiomics profiling stratified nonviral HCCs according to prognosis or the TIME. We further identified the link between intratumoral steatosis and immune-exhausted immunotherapy-susceptible TIME in HCC.

AUTHOR CONTRIBUTIONS

Hiroki Murai: data curation, formal analysis, validation, visualization, and writing original draft. Takahiro Kodama: conceptualization, formal analysis, funding acquisition, validation, visualization, and writing original draft. Kazuki Maesaka: formal analysis. Shoichiro Tange: formal analysis and writing original draft. Daisuke Motooka: formal analysis and writing original draft. Yutaka Suzuki: formal analysis and writing original draft. Yasuyuki Shigematsu: resources and data curation. Kentaro Inamura: resources and data curation. Yoshihiro Mise: resources and data curation. Akio Saiura: resources and data curation. Yoshihiro Ono: resources and data curation. Yu Takahashi: resources and data curation. Yota Kawasaki: resources and data curation. Satoshi Iino: resources and data curation. Shogo Kobayashi: resources and data curation. Masashi Idogawa: formal analysis. Takashi Tokino: formal analysis. Tomomi Hashidate-Yoshida: formal analysis and writing the original draft. Hideo Shindou: formal analysis. Masanori Miyazaki: resources and data curation. Yasuharu Imai: resources and data curation. Satoshi Tanaka: resources and data curation. Eiji Mita: resources and data curation. Kazuyoshi Ohkawa: resources and data curation. Hayato Hikita: methodology. Ryotaro Sakamori: methodology. Tomohide Tatsumi: methodology. Hidetoshi Eguchi: methodology. Eiichi Morii: methodology and formal analysis. Tetsuo Takehara: conceptualization, formal analysis, funding

acquisition, supervision, and writing, review, and editing.

ACKNOWLEDGMENTS

This work was supported by JSPS KAKENHI Grant Number 16H06279 (PAGS).

CONFLICT OF INTEREST

Hayato Hikita, Takahiro Kodama and Tetsuo Takehara are on the speakers' bureau for Chugai Pharmaceutical Co., Ltd.

DATA DEPOSITION

The RNA-seq data reported in this study have been deposited in the Gene Expression Omnibus database under the following accession number: GSE190967.

The Genome-seq data reported in this study have been deposited in the Japanese Genotype–phenotype Archive (JGA) under the following accession numbers: JGAS000523 and JGAD000642.

The spatial transcriptomics data reported in this study have been deposited in the JGA under the following accession number: JGAS000311.

ORCID

Takahiro Kodama https://orcid.org/0000–0002–6250–1324
Kentaro Inamura https://orcid.org/0000–0001–6444–3861
Ryotaro Sakamori https://orcid.org/0000–0002–1580–607X

REFERENCES

1. Bray F, Ferlay J, Soerjomataram I, Siegel RL, Torre LA, Jemal A. Global cancer statistics 2018: GLOBOCAN estimates of incidence and mortality worldwide for 36 cancers in 185 countries. CA Cancer J Clin. 2018;68:394–424. doi: 10.3322/caac.21492
2. Paradis V. Histopathology of hepatocellular carcinoma. Recent Results Cancer Res. 2013;190:21–32.
3. Kanwal F, Singal AG. Surveillance for hepatocellular carcinoma: current best practice and future direction. Gastroenterology. 2019;157:54–64.
4. Cazzagon N, Trevisani F, Maddalo G, Giacomin A, Vanin V, Pozzan C, et al. Rise and fall of HCV-related hepatocellular carcinoma in Italy: a long-term survey from the ITA.LI.CA centres. Liver Int. 2013;33:1420–7.
5. Hamed MA, Ali SA. Non-viral factors contributing to hepatocellular carcinoma. World J Hepatol. 2013;5:311–22.
6. Schulze K, Imbeaud S, Letouzé E, Alexandrov LB, Calderaro J, Rebouissou S, et al. Exome sequencing of hepatocellular carcinomas identifies new mutational signatures and potential therapeutic targets. Nat Genet. 2015;47:505–11.
7. Hoshida Y, Nijman SMB, Kobayashi M, Chan JA, Brunet JP, Chiang DY, et al. Integrative transcriptome analysis reveals common molecular subclasses of human hepatocellular carcinoma. Cancer Res. 2009;69:7385–92.
8. Chiang DY, Villanueva A, Hoshida Y, Peix J, Newell P, Minguez B, et al. Focal gains of VEGFA and molecular classification of hepatocellular carcinoma. Cancer Res. 2008;68:6779–88.
9. Pinyol R, Torrecilla S, Wang H, Montironi C, Piqué-Gili M, Torres-Martin M, et al. Molecular characterisation of hepatocellular carcinoma in patients with non-alcoholic steatohepatitis. J Hepatol. 2021;75:865–78.
10. Kyi C, Postow MA. Immune checkpoint inhibitor combinations in solid tumors: Opportunities and challenges. Immunotherapy. 2016;8:821–37.
11. Finn RS, Qin S, Ikeda M, Galle PR, Ducreux M, Kim TY, et al. Atezolizumab plus bevacizumab in unresectable hepatocellular carcinoma. N Engl J Med. 2020;382:1894–905.
12. Rebouissou S, Nault JC. Advances in molecular classification and precision oncology in hepatocellular carcinoma. J Hepatol. 2020;72:215–9.
13. Sia D, Jiao Y, Martinez-Quetglas I, Kuchuk O, Villacorta-Martin C, Castro de Moura M, et al. Identification of an immune-specific class of hepatocellular carcinoma, based on molecular features. Gastroenterology. 2017;153:812–26.
14. Li F, Li C, Cai X, Xie Z, Zhou L, Cheng B, et al. The association between CD8+ tumor-infiltrating lymphocytes and the clinical outcome of cancer immunotherapy: a systematic review and meta-analysis. EClinicalMedicine. 2021;41:101134.
15. Lu S, Stein JE, Rimm DL, Wang DW, Bell JM, Johnson DB, et al. Comparison of biomarker modalities for predicting response to PD-1/PD-L1 checkpoint blockade: a systematic review and meta-analysis. JAMA Oncol. 2019;5:1195–204.
16. Pfister D, Nunez NG, Pinyol R, Govaere O, Pinter M, Szydlowska M, et al. NASH limits anti-tumour surveillance in immunotherapy-treated HCC. Nature. 2021;592:450–6.
17. Kozumi K, Kodama T, Murai H, Sakane S, Govaere O, Cockell S, et al. Transcriptomics identify thrombospondin-2 as a biomarker for nonalcoholic steatohepatitis and advanced liver fibrosis. Hepatology. 2021;74:2452–66.
18. Cassidy FH, Yokoo T, Aganovic L, Hanna RF, Bydder M, Middleton MS, et al. Fatty liver disease: MR imaging techniques for the detection and quantification of liver steatosis. Radiographics. 2009;29:231–60.
19. Kodama T, Yi J, Newberg JY, Tien JC, Wu H, Finegold MJ, et al. Molecular profiling of nonalcoholic fatty liver disease-associated hepatocellular carcinoma using SB transposon mutagenesis. Proc Natl Acad Sci U S A. 2018;115:E10417–26.
20. Kodama T, Takehara T, Hikita H, Shimizu S, Li W, Miyagi T, et al. Thrombocytopenia exacerbates cholestasis-induced liver fibrosis in mice. Gastroenterology. 2010;138:2487–98, 2498.e1–7.
21. Ally A, Balasundaram M, Carlsen R, Chuah E, Clarke A, Dhalla N, et al. Comprehensive and integrative genomic characterization of hepatocellular carcinoma. Cell. 2017;169:1327–41.e23.
22. Pinyol R, Sia D, Llovet JM. Immune exclusion-Wnt/CTNNB1 class predicts resistance to immunotherapies in HCC. Clin Cancer Res. 2019;25:2021–3.
23. Quigley M, Pereyra F, Nilsson B, Porichis F, Fonseca C, Eichbaum Q, et al. Transcriptional analysis of HIV-specific CD8(+) T cells shows that PD-1 inhibits T cell function by upregulating BATF. Nat Med. 2010;16:1147–51.
24. Yoshihara K, Shahmoradgoli M, Martinez E, Vegesna R, Kim H, Torres-Garcia W, et al. Inferring tumour purity and stromal and immune cell admixture from expression data. Nat Communi. 2013;4:2612.
25. Thommen DS, Schumacher TN. T cell dysfunction in cancer. Cancer Cell. 2018;33:547–62.
26. Stephen TL, Rutkowski MR, Allegrezza MJ, Perales-Puchalt A, Tesone AJ, et al. Transforming growth factor β-mediated suppression of antitumor T cells requires FoxP1 transcription factor expression. Immunity. 2014;41:427–39.
27. Zhang M, Huang L, Ding G, Huang H, Cao G, Sun X, et al. Interferon gamma inhibits CXCL8-CXCR2 axis mediated tumor-associated macrophages tumor trafficking and enhances anti-PD1 efficacy in pancreatic cancer. J Immunother. Cancer. 2020;8:e000308.

28. Zhang F, Wang HS, Wang XF, Jiang GM, Liu H, Zhang G, et al. TGF-β induces M2-like macrophage polarization via SNAIL-mediated suppression of a pro-inflammatory phenotype. Oncotarget. 2016;7:52294–306.
29. Braza MS, Conde P, Garcia M, Cortegano I, Brahmachary M, Pothula V, et al. Neutrophil derived CSF1 induces macrophage polarization and promotes transplantation tolerance. Am J Transplant. 2018;18:1247–55.
30. Hoshida Y, Toffanin S, Lachenmayer A, Villanueva A, Minguez B, Llovet JM. Molecular classification and novel targets in hepatocellular carcinoma: Recent advancements. Semin Liver Dis. 2010;30:35–51.
31. Zucman-Rossi J, Villanueva A, Nault JC, Llovet JM. Genetic landscape and biomarkers of hepatocellular carcinoma. Gastroenterology. 2015;149:1226–39.e4.
32. Llovet JM, Villanueva A, Lachenmayer A, Finn RS. Advances in targeted therapies for hepatocellular carcinoma in the genomic era. Nat Rev Clin Oncol. 2015;12:408–24.
33. Zhang Y, Sun Y, Rao E, Yan F, Li Q, Silverstein KAT, et al. Fatty acid-binding protein E-FABP restricts tumor growth by promoting IFN-β responses in tumor-associated macrophages. Cancer Res. 2014;74:2986–98.
34. den Brok MH, Büll C, Wassink M, de Graaf AM, Wagenaars JA, Minderman M, et al. Saponin-based adjuvants induce cross-presentation in dendritic cells by intracellular lipid body formation. Nat Commun. 2016;7:13324.
35. Al-Khami AA, Zheng L, Del Valle L, Hossain F, Wyczechowska D, Zabaleta J, et al. Exogenous lipid uptake induces metabolic and functional reprogramming of tumor-associated myeloid-derived suppressor cells. Onco Targets Ther. 2017;6:e1344804.
36. Niu Z, Shi Q, Zhang W, Shu Y, Yang N, Chen B, et al. Caspase-1 cleaves PPARγ for potentiating the pro-tumor action of TAMs. Nat Commun. 2017;8:766.
37. Veglia F, Tyurin VA, Mohammadyani D, Blasi M, Duperret EK, Donthireddy L, et al. Lipid bodies containing oxidatively truncated lipids block antigen cross-presentation by dendritic cells in cancer. Nat Commun. 2017;8:2122.
38. Wu H, Han Y, Rodriguez Sillke Y, Deng H, Siddiqui S, Treese C, et al. Lipid droplet-dependent fatty acid metabolism controls the immune suppressive phenotype of tumor-associated macrophages. EMBO Mol Med. 2019;11:e10698.
39. Calderaro J, Couchy G, Imbeaud S, Amaddeo G, Letouzé E, Blanc JF, et al. Histological subtypes of hepatocellular carcinoma are related to gene mutations and molecular tumour classification. J Hepatol. 2017;67:727–38.
40. Salomao M, Remotti H, Vaughan R, Siegel AB, Lefkowitch JH, Moreira RK. The steatohepatitic variant of hepatocellular carcinoma and its association with underlying steatohepatitis. Hum Pathol. 2012;43:737–46.
41. Yau T, Kang YK, Kim TY, El-Khoueiry AB, Santoro A, Sangro B, et al. Efficacy and safety of nivolumab plus ipilimumab in patients with advanced hepatocellular carcinoma previously treated with sorafenib: The CheckMate 040 Randomized Clinical Trial. JAMA Oncol. 2020;6:e204564.

How to cite this article: Murai H, Kodama T, Maesaka K, Tange S, Motooka D, Suzuki Y, et al. Multiomics identifies the link between intratumor steatosis and the exhausted tumor immune microenvironment in hepatocellular carcinoma. Hepatology. 2023;77:77–91. https://doi.org/10.1002/hep.32573